Supporting Information

Evolution of Metal Selectivity in Templated Protein Interfaces

Jeffrey D. Brodin[†], Annette Medina-Morales[†], Thomas Ni[†], Eric N. Salgado[†], Xavier I. Ambroggio[‡], and F. Akif Tezcan[†]*

[†]*Department of Chemistry and Biochemistry, University of California, San Diego, La Jolla, CA 92093-0356;* [‡]*Rosetta Design Group LLC, Fairfax, VA 22030*

This file contains Supporting Table S1, DynaFit scripts, Supporting Figures S1-11.

Table S1. X-ray data collection and refinement statistics. (* denotes highest resolution shell).

	^{96C}RIDC-1$_4$	Zn$_4$:^{96C}RIDC-1$_4$	Cu/Zn$_4$:^{96C}RIDC-1$_4$
Data collection location	SSRL BL 9-2	SSRL BL 9-2	SSRL BL 7-1
Unit cell dimensions (Å)	69.2 x 69.2 x 186.9 $\alpha = \beta = \gamma = 90°$	63.3 x 76.8 x 177.6 $\alpha = \beta = \gamma = 90°$	63.5 x 78.1 x 178.3 $\alpha = \beta = \gamma = 90°$
Symmetry group	$I4_1$	$P2_12_12_1$	$P2_12_12_1$
Resolution (Å)	46.3 – 2.05	88.8 – 2.35	89.2 – 2.10
X-ray wavelength (Å)	0.98	0.98	1.00
Number of unique reflections	27287	36701	49272
Redundancy	5.0	4.0	9.5
Completeness (%)*	99.6 (100)	99.5 (99.9)	93.6 (84.2)
$\langle I / \sigma I \rangle$*	10.8 (1.5)	4.9 (1.8)	4.0 (1.5)
R_{symm}* (%)	8.0 (44.8)	9.8 (35.6)	10.2 (17.6)
R_{work}/R_{free} (%)	22.9 / 27.7	22.8 / 29.6	22.5 / 27.1
Number of atoms			
Protein	3272	6544	6544
Ligands/ions	171	352	352
Water	236	145	395
B-factors (Å^2)			
Protein	37.2	47.0	27.2
Ligands/ions	30.1	41.9	27.0
Water	42.4	42.4	31.4
R.m.s deviations			
Bond lengths (Å)	0.015	0.016	0.009
Bond angles (°)	1.46	1.37	1.01

DynaFit Scripts

Titration of Fura-2 in the presence of EGTA. This script describes the competition between Fura-2 and EGTA for binding to M^{2+} (Zn^{2+} in this example) used to determine the binding constants for Fura-2 metal binding.

```
[task]
task = fit
data = equilibria

; L ... Fura-2
; E ... EGTA
; M ... Zn

[mechanism]
L + M <==> LM : Kd1 dissoc
E + M <==> EM : Kd2 dissoc

[constants]
Kd1 = 3e-9 ?
Kd2 = 8.1e-9

[concentrations]
L = 10.4e-6

[responses]
L = 27000 ?
LM = 9000 ?

[equilibria]
directory ./data_directory
extension txt
variable M
file data_file          |       concentration E = 93.9e-6

[output]
directory ./output_directory
```

Fura-2 vs. ^{C96}RIDC-1_4 for four consecutive binding equilibria. This script describes the competition between Fura-2 and ^{C96}RIDC-1_4 for Zn^{2+}. Scripts similar to this one were used to fit one and two consecutive zinc binding equilibria, as well as both models for Ni^{2+} and Cu^{2+}. See note below for modifications used to fit other models.

```
[task]
task = fit
data = equilibria

; L ... Fura-2
; P ... 96C
; M ... Zn - competing ligand

[mechanism]
L + M <==>   LM : Kd1 dissoc
P + M  <==>   PM : Kd2 dissoc
PM + M <==> PMM : Kd3 dissoc
PMM + M <==> PMMM : Kd4 dissoc
PMMM + M <==> PMMMM : Kd5 dissoc

[constants]
Kd1 = 5.7e-9
Kd2 = 3e-9 ?
Kd3 = 2e-8 ?
Kd4= 3e-8?
Kd5= 7e-8 ?

[concentrations]
L = 10e-6

[responses]
L = 27000 ?
LM = 9000 ?

[equilibria]
directory ./data_directory
extension txt
variable M
file data_file              |          concentration P = 30e-6

[output]
directory ./output_directory
```

Notes on other models:

1) *Zn – 2 consecutive equilibria*: To account for two binding equilbria, each of which represents the association of two Zn^{2+}, the concentration of protein was doubled relative to the above model. The equilibrium expressions are reduced to

L + M <==> LM : Kd1 dissoc
P + M <==> PM : Kd2 dissoc
PM + M <==> PMM : Kd3 dissoc

2) *Zn – 1 equilibrium:* The concentration of protein was quadrupled and the following equilibria were used

L + M <==> LM : Kd1 dissoc
P + M <==> PM : Kd2 dissoc

3) *Ni and Cu – 2 consecutive equilibria:* The concentration of protein was set to the tetramer concentration and the equilibrium expressions outlined in note 1 were used.

4) *Ni and Cu – 1 equilibrium:* The concentration of protein was set to half the tetramer concentration and the equilibrium expressions outlined in note 2 were used.

Supporting Figures

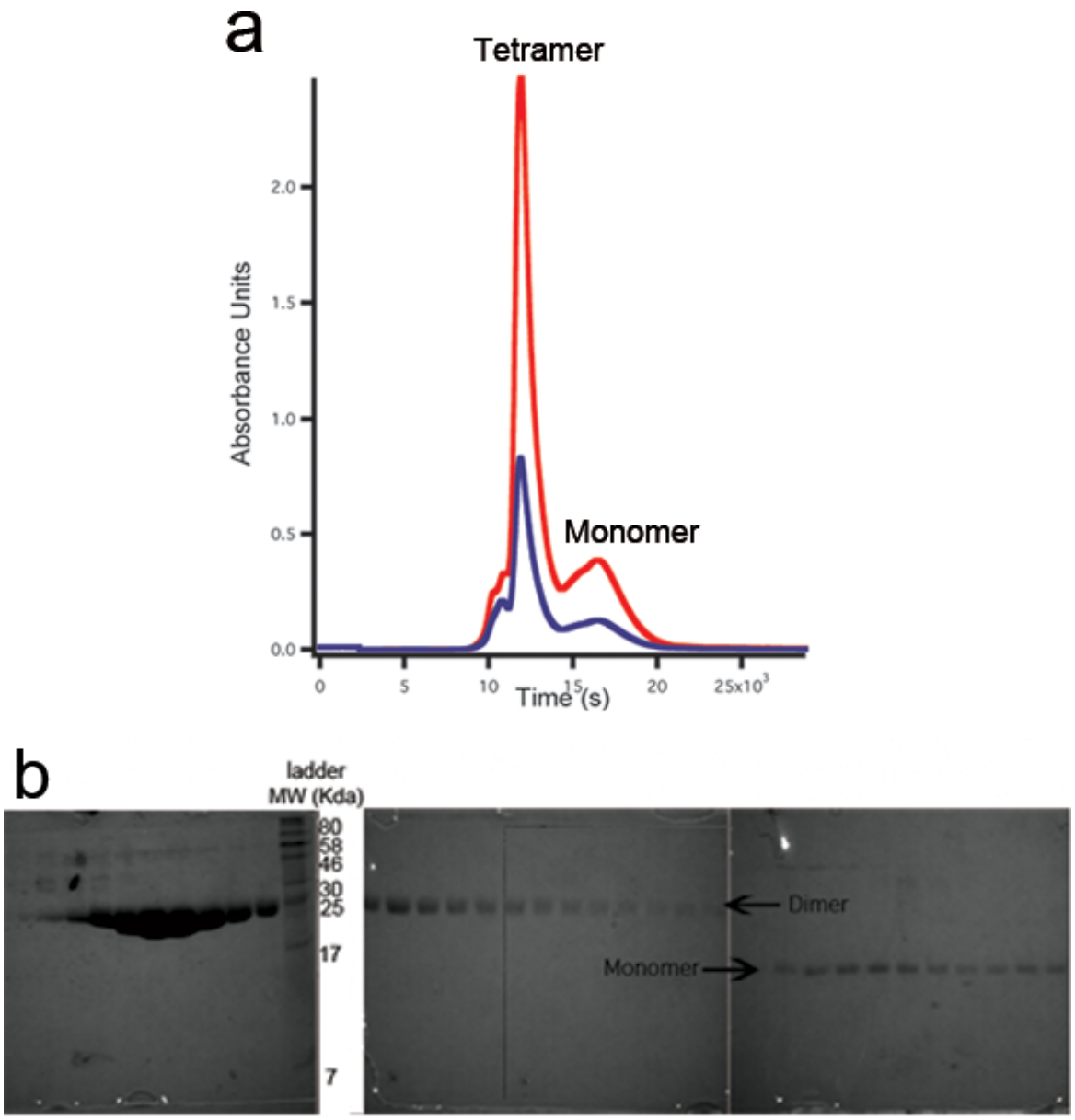

Figure S1. Purification and characterization of disulfide crosslinked ^{C96}RIDC-1 (^{C96}RIDC-1$_2$). (a) Size-exclusion chromatogram of air-oxidized ^{96C}RIDC-1. The lack of distinct peaks for dimer and tetramer is likely due to the high loading concentrations, resulting in complete tetramer formation. (b) Non-reducing, denaturing SDS-PAGE gels of fractions collected from SEC.

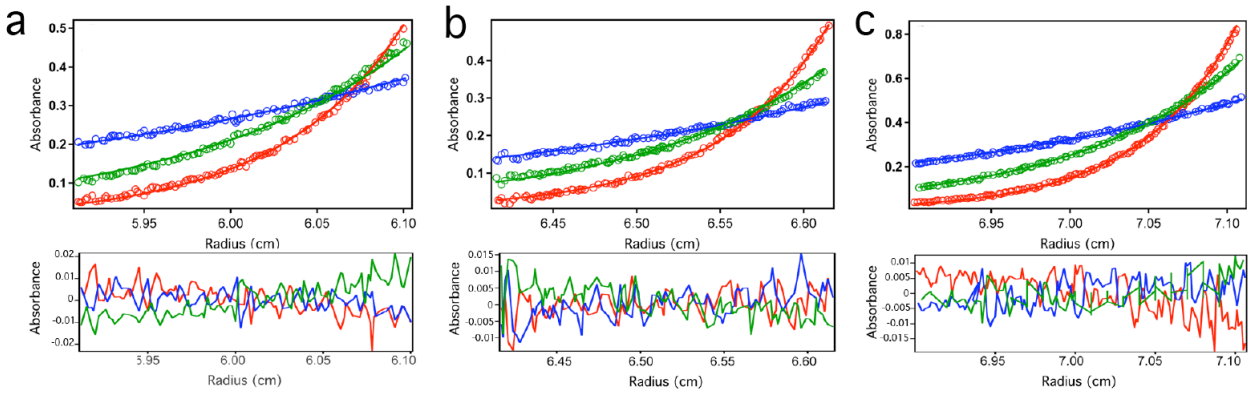

Figure S2. Sedimentation equilibrium (SE) profiles for ^{C96}RIDC-1. (a) 1 μM ^{C96}RIDC-1_2 at 10000, 15000 and 20000 rpm. (b) 2.5 μM ^{C96}RIDC-1_2 at 10000, 15000 and 20000 rpm. (c) 12.5 μM ^{C96}RIDC-1_2 at 10000, 15000 and 20000 rpm. All samples contain 20 mM Tris (pH 7), 150 mM NaCl and 5 mM EDTA and were run at 25^{o} C. Scans shown here were globally fit to a dimer-tetramer model.

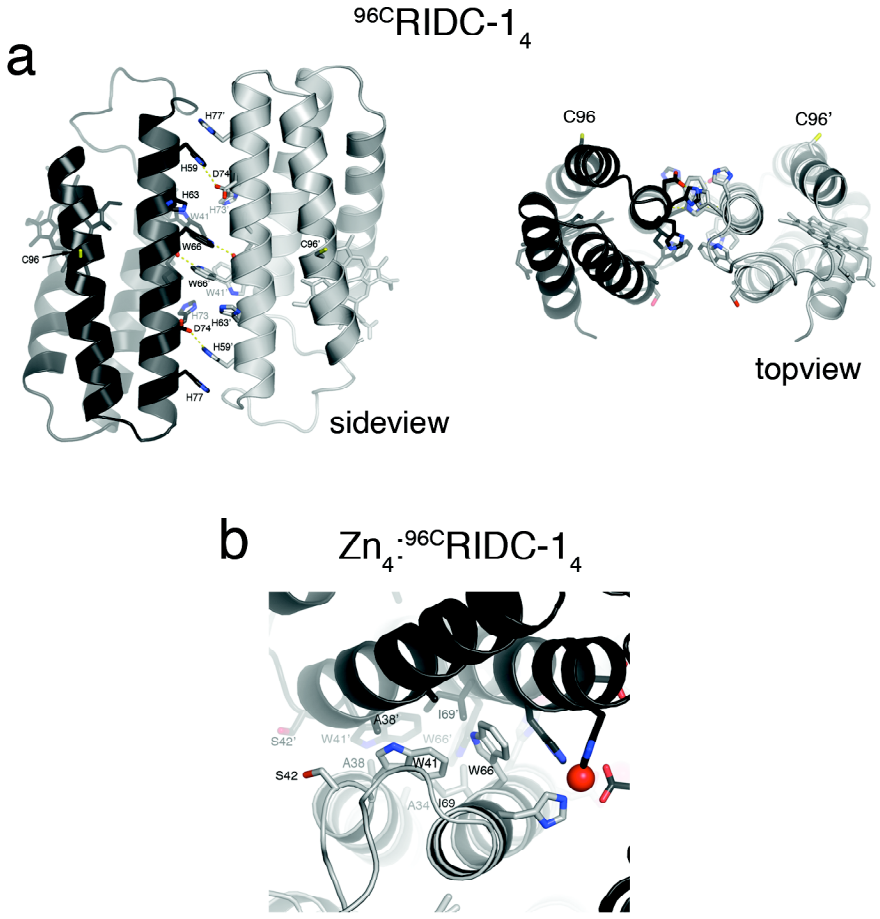

Figure S3. Interactions between engineered residues in interfaces *i1* and *i2*. (a) ^{C96}RIDC-1_4; (b) Zn_4:^{C96}RIDC-1_4.

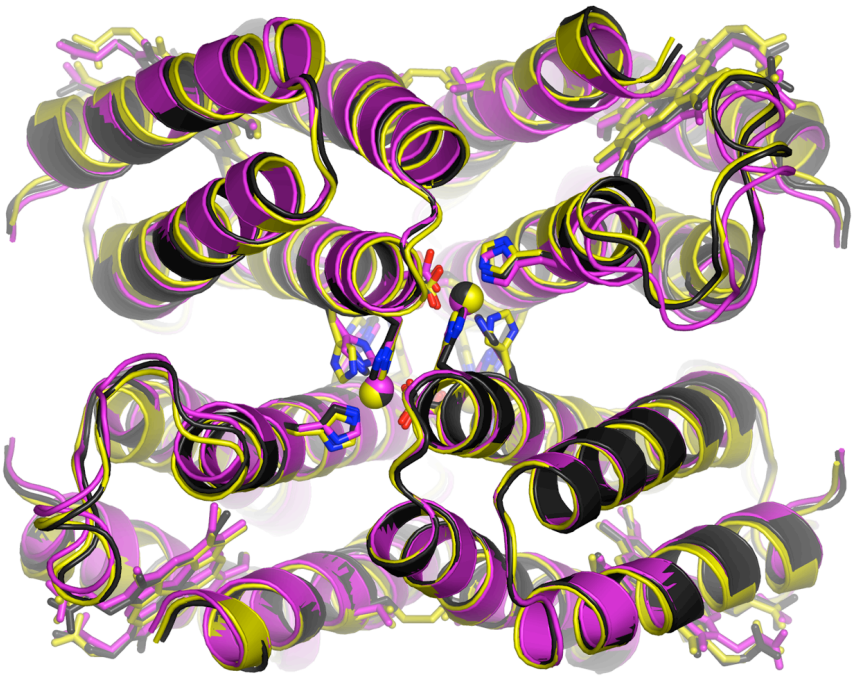

Figure S4. Superposition of Zn_4:MBPC-1_4 (yellow), Zn_4:RIDC-1_4 (magenta) and Zn_4:^{C96}RIDC-1_4 (grey) crystal structures.

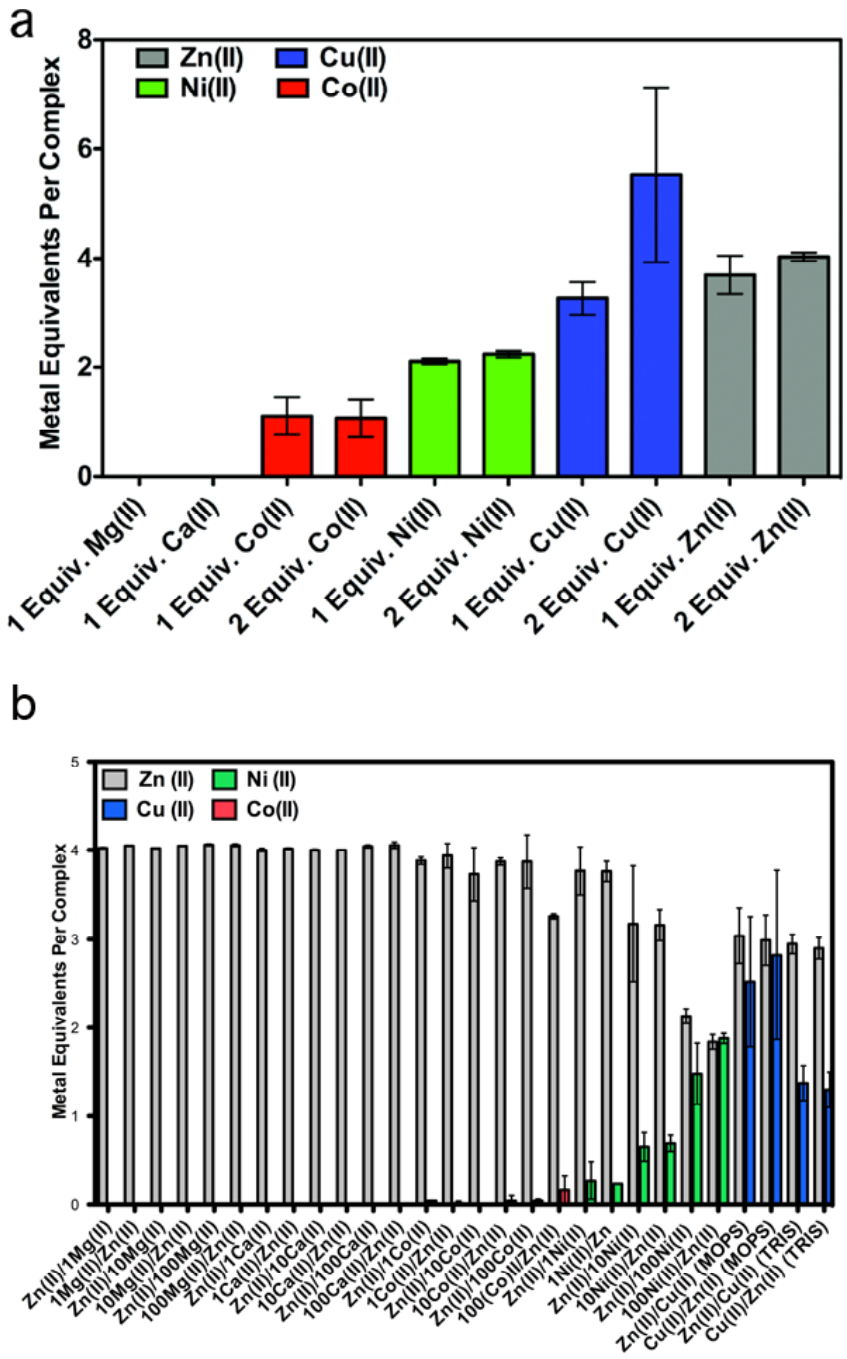

Figure S5. Divalent metal binding properties of ^{C96}RIDC-1_4. (a) Equivalents of M^{2+} bound to ^{C96}RIDC-1_4 following size exclusion chromatography, as determined by ICP-OES measurements (in 20 mM MOPS buffer). The protein concentration was determined using the single heme Fe of each RIDC-1 monomer as an internal standard. (b) Complete Zn^{2+} versus M^{2+} competition binding assay for ^{C96}RIDC-1_4 binding (in 20 mM MOPS buffer or in 20 mM TRIS where indicated). This plot includes metal competition assays carried out in both directions (incubation with Zn^{2+} followed by M^{2+}, or incubation with M^{2+} followed by Zn^{2+}). The results show that the metal content is the same in both directions in each case, indicating that metal binding to ^{C96}RIDC-1_4 is under thermodynamic control under the conditions employed.

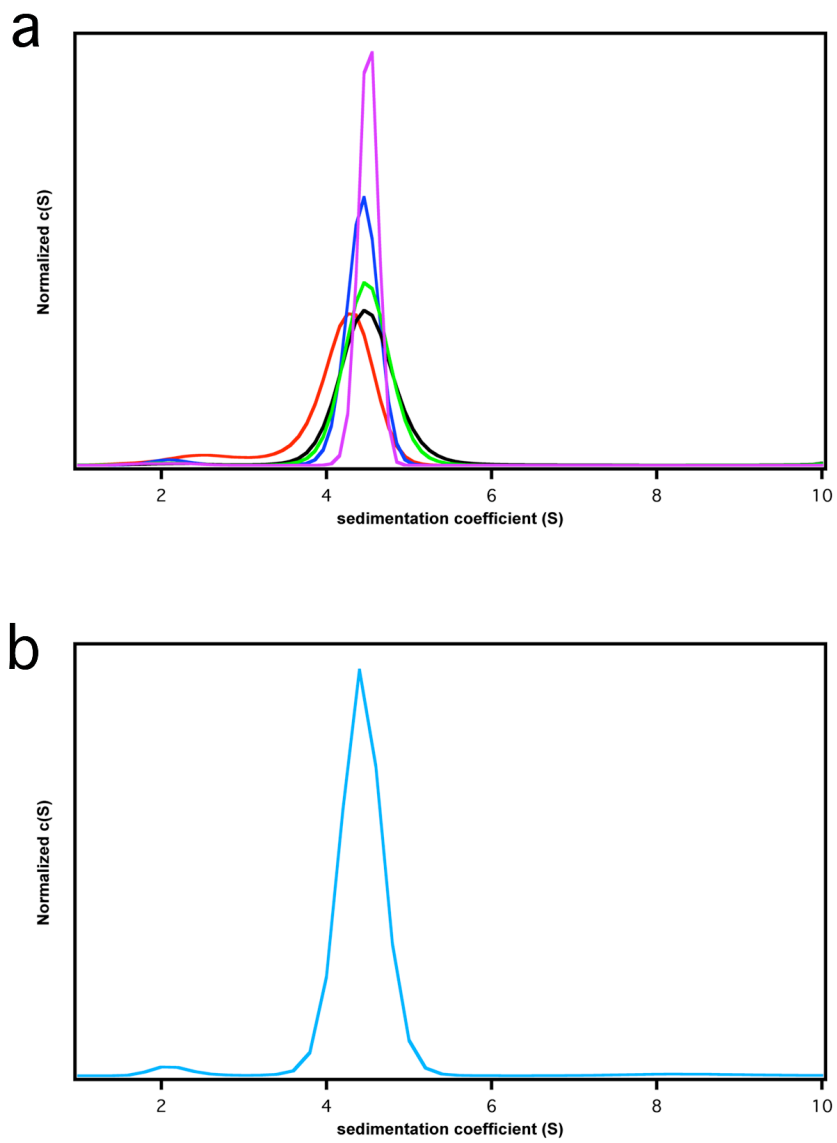

Figure S6. Sedimentation coefficient distributions for ^{C96}RIDC-1 in the presence and absence of metals, showing the formation of tetrameric forms at all conditions. (a) (red trace) 2.5 μM ^{C96}RIDC-1_2 + 5 mM EDTA ; (green trace) 2.5 μM ^{C96}RIDC-1_2 + 5 μM Zn; (black trace) 2.5 μM ^{C96}RIDC-1_2 + 5 μM Cu; (blue trace) 2.5 μM ^{C96}RIDC-1_2 + 5 μM Co; (purple trace) 15 μM ^{C96}RIDC-1_2 and 30 μM Ni. (b) 15 μM ^{C96}RIDC-1_2 + 30 μM Zn (initial) + 30 μM Cu (initial). This sample was run down a gel-filtration column following incubation with metals in a manner analogous to competition experiments.

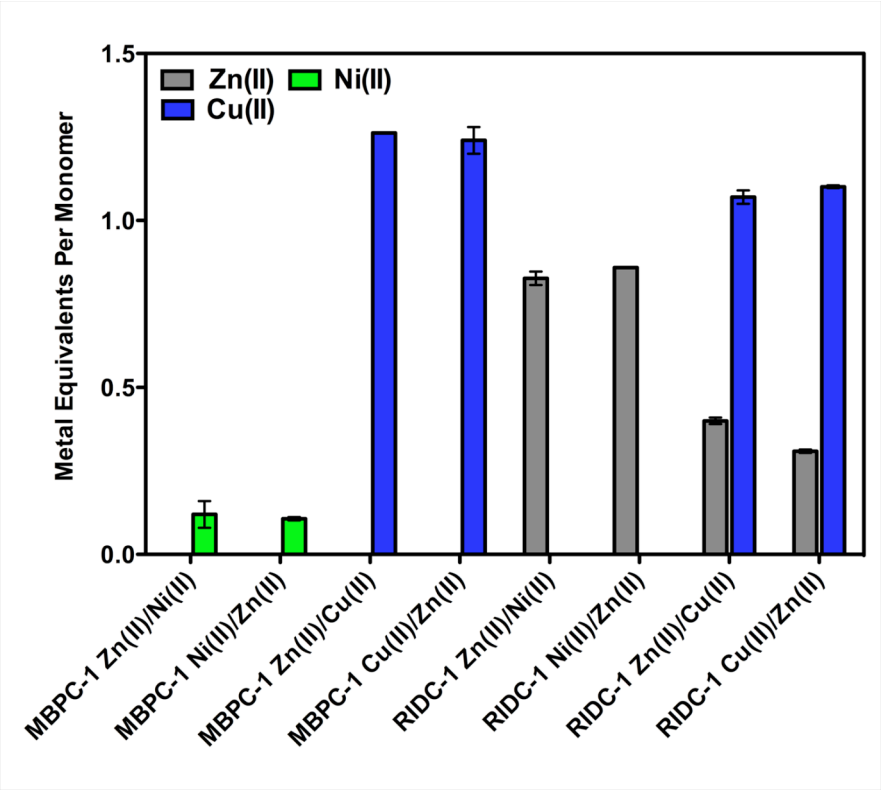

Figure S7. Zn^{2+} versus M^{2+} competition binding assay for MBPC-1 and RIDC-1. These experiments were performed in an identical fashion as those for metal binding to ^{C96}RIDC-1_4. Note that the y-axis reports metal equivalents per monomer instead of tetramer, since MBPC-1 and RIDC-1 do not form persistent tetramers without metal. These competition binding experiments show that both Ni^{2+} and Cu^{2+} outcompete Zn^{2+} for MBPC-1 binding. In the case of RIDC-1, Cu^{2+} still outcompetes Zn^{2+} (though not to the same extent as MBPC-1).

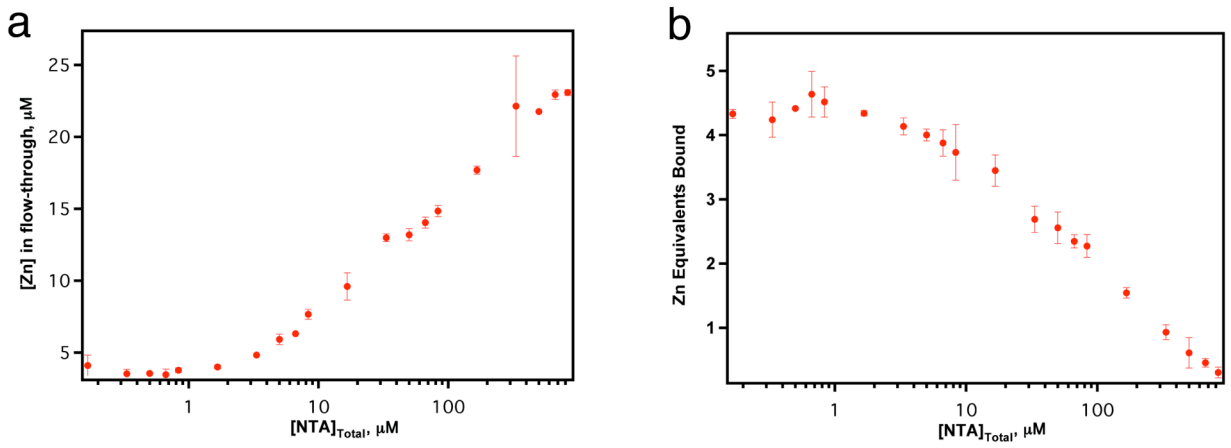

Figure S8. Raw data for the determination of Zn binding affinity to ^{C96}RIDC-1$_4$ using PAR as an indicator (see experimental section for details). (a) Concentration of Zn(II) in flow-through, and (b) Zn equivalents bound to ^{C96}RIDC-1$_4$ as a function of added NTA. A rough estimate for the Zn-^{C96}RIDC-1$_4$ dissociation constant can be made based on the NTA concentration, at which 50% of binding sites are occupied. b shows that 22 µM ^{C96}RIDC-1$_4$ is half Zn-bound at ~100 µM NTA, yielding a dissociation constant of ~3 nM based on a Zn-NTA dissociation constant of 15 nM. This value is in good agreement with the value of 3.3 nM determined by plotting free Zn concentration versus Zn equivalents per tetramer (Figure 4a).

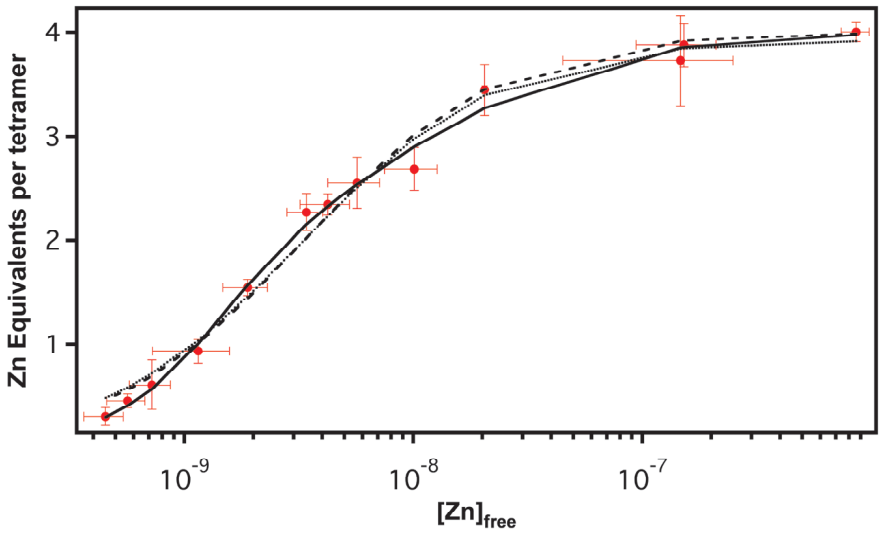

Figure S9. Zn-binding isotherm of ^{C96}RIDC-1_4 determined using NTA as a competing ligand. The fits obtained using DynaFit are shown for the following different models: solid line, four consecutive Zn binding equilibria (1+1+1+1); dashed line, two consecutive binding equilibria (2+2); dotted line; single binding equilibrium (4×1). The mathematical expressions used for these models can be found in the Experimental Section. The obtained dissociation constants are as follows. 4×1 model: 3.3(3) nM; 2+2 model: 2.0(3) and 6(1) nM; 1+1+1+1 model: 3(3) nM, 0.8(8) nM, 5(3) nM and 30(10) nM.

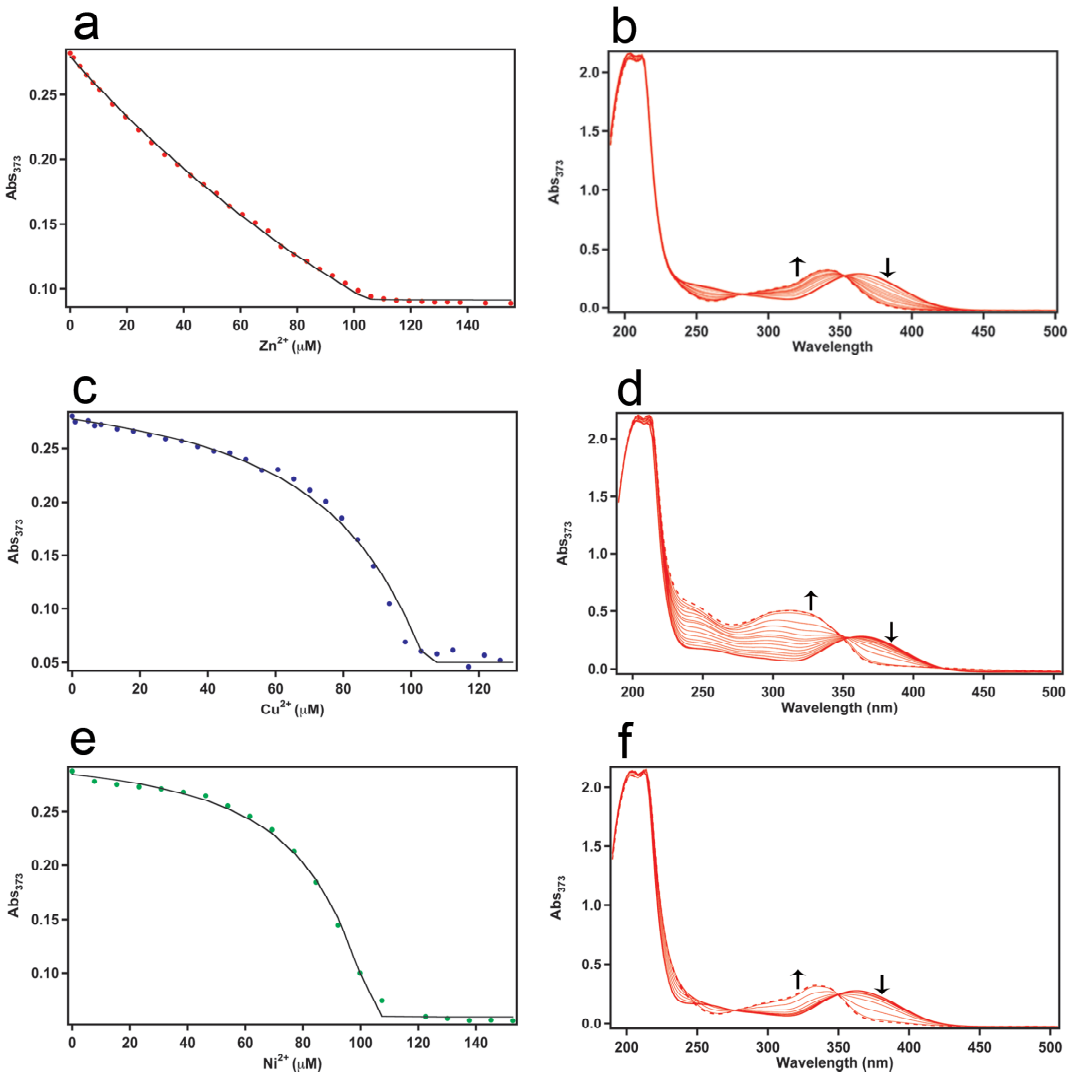

Figure S10. Metal binding isotherms and UV-vis spectra for Fura-2-EGTA competition binding experiments. (a) Binding isotherm for 11 μM Fura-2 and 94 μM EGTA titrated with Zn^{2+}. (b) UV-vis spectra corresponding to individual points in (a). (c) Binding isotherm for 11 μM fura-2 and 94 μM EGTA titrated with Cu^{2+}. (d) UV-vis spectra corresponding to individual points in (c). (e) Binding isotherm for 11 μM fura-2 and 94 μM EGTA titrated with Ni^{2+}. (f) UV-vis spectra corresponding to individual points in (e). All titrations were fit to 1:1 M^{2+}:Fura-2 and 1:1 M^{2+}:EGTA using DynaFit.

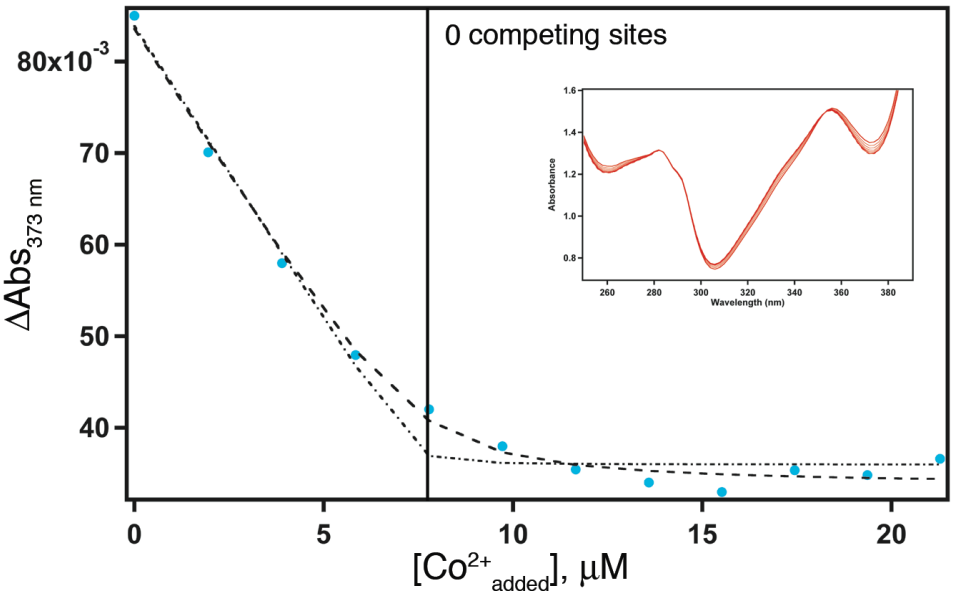

Figure S11. Co^{2+} binding isotherm for Fura-2–^{C96}RIDC-1_4 competition experiments; corresponding changes in the Fura-2 absorbance spectrum are shown in the inset. The samples contained 21 μM ^{C96}RIDC-1_4 and 8 μM Fura-2. The titration shows that there is only one apparent site on ^{C96}RIDC-1_4 that is barely able to compete with Fura-2 for Co^{2+} binding, yielding a dissociation constant of 0.9 μM.